2021 IEEE 4th International Conference on Soft Robotics (RoboSoft)
April 12-16, 2021, Yale University, USA

Fabrication and Characterization of I-cord Knitted SMA Actuators

Christopher Kim, Athena Chien, Megha Tippur, Cynthia Sung

2021 IEEE 4th International Conference on Soft Robotics (RoboSoft) | 978-1-7281-7713-7/20/$31.00 ©2021 IEEE | DOI: 10.1109/RoboSoft51838.2021.9479207

Abstract— **Knitted SMA actuators provide greater actuation stroke than single-strand SMA wire actuators by leveraging its knitted structure. However, due to short-circuiting through interlacing knit loops, existing knitted SMA sheet actuators are unsuitable for joule-heating actuation when uniform contractile actuation is desired. We explore an axially symmetric tubular i-cord knitted actuator as a possible solution. The fabrication process of an i-cord knitted SMA actuator and its electrical, thermal, and mechanics models are presented. After modifying existing models for single-strand SMA wire and adjusting their parameters, the proposed electrical, thermal, and mechanics models were verified with experimental results.**

I. Introduction

Embedding smart materials, such as SMA [1]–[3], electroactive polymers [4], or dielectric elastomers [5], in composite-made soft robots provides multiple advantages because they not only act as actuator units to mimic a muscular function, but also form the supporting parts of the soft structure [6]. SMA, in particular, leverages the strain which arises from its own phase change between martensite and austenite phases. Knitting SMA wires not only converts SMA wires into planar or three-dimensional geometries, but also generates greater strain [7]. Recently, applications of knitted SMA actuators have also been demonstrated especially in self-fitting wearable devices [8], [9].

A. Shape Memory Alloy (SMA) as Actuators

Shape Memory Alloy (SMA) actuators utilize the shape memory effect of certain metal alloys which, once deformed in martensite state, return to their original undeformed length in austenite state when heated. The most popular shape memory alloy is NiTi (nickel titanium) because of its favorable material properties, non-toxicity, and reasonable cost [10]. In the martensite phase, NiTi has low crystal symmetry and can be easily deformed plastically with relatively low stress. Once it is heated above its phase transition temperature, NiTi has a more symmetric crystalline structure in its austenite phase and it returns to having the same distribution of atoms as before the plastic deformation [11].

Through shape memory effect, strains up to 8% can be recovered by a NiTi wire, providing useful actuator capabilities [12]. By simply passing an electric current though the NiTi wire, the temperature of the NiTi wire can be increased through Joule heating. Compared to other soft actuators and smart materials which have been developed with varying fabrication methods and capabilities, SMA actuators have a high power density and require minimal control infrastructure [13], [14], resulting in multiple examples of SMA actuators being used in robotics for application such as microgrippers, mobile robots, surgical robots, and aerial vehicles [15]–[22].

B. Modeling SMA Actuators

Since the discovery of the R-phase in the early 90s, there has been various attempts to mathematically model both the mechanical and thermoeleastic properties of NiTi [23], [24]. However, the relationship between current delivered and desired displacement is highly nonlinear because the change in temperature causes a phase change between the austenite and martensite phases, resulting in hysteresis. While knowing the instantaneous martensite or austenite fractions would enable direct extrapolation to the resulting displacement, this is only possible through a destructive physical analysis [25]. Instead, in order to leverage the strengths of NiTi wire for actuation, a hysteresis model relating martensite fraction to temperature and its corresponding stress-strain relationship was developed to integrate with a proportional-integral-derivative (PID) or pulse-width modulated (PWM) control [26]. The model from [25] builds on this to suggest a differential hysteresis model of spring-biased NiTi wire: relating martensite fraction with strain, temperature, and resistance. It has also been shown that by utilizing a Direct Adaptive Controller and a Kalmann Filter estimator on this differential hysteresis model to compensate for hysteresis, a more effective controller for NiTi wire can be developed than conventional PIDs [27].

C. Knitted SMA Actuators

Early studies in contractile knitted SMA actuators have shown that leveraging a hierarchical knitted structure can increase contraction to up to 50% the original length, even under high applied loads between 1N to 10N [7]. These results highly depend on geometric parameters such as wire diameter and loop-enclosed area [28]. There also have been efforts to quantify the characteristic performance of knitted NiTi actuators by measuring the austenite phase fraction of a knitted NiTi architecture under different positions and thermo-mechanical loading conditions using x-ray micro-diffraction analysis [29]. Given these results, smart fabric textiles using SMA have found their way into robotic applications including robotic fabrics actuated by antagonistic pairs

C. Kim and C. Sung are with the General Robotics, Automation, Sensing & Perception (GRASP) Lab at the University of Pennsylvania, Philadelphia, PA, USA. (emails: cyoonjae@seas.upenn.edu, crsung@seas.upenn.edu) A. Chien is with the Department of Bioengineering, Rice University, Houston, TX, USA. (email: ajc13@rice.edu). M. Tippur is with the Computer Science & Artificial Intelligence Lab (CSAIL) at Massachusetts Institute of Technology, Cambridge, MA, USA. (email: mhtippur@mit.edu).

Support for this project has been provided in part by NSF REU EEC-1659190 and by the GeorgiaTech Stamps President's Scholars program.

of SMA ribbons [30], woven rolling robots [31], and soft robotic flowers [32]. The high percent-actuation contractions of knitted SMA technology has even been harnessed to prototype a self-fitting, variable-stiffness garment for potential uses in wearable robots and health monitoring devices [8].

D. Contributions

Various physical characteristics of SMA can depend on the temperature at which NiTi was heat-treated during its manufacturing process [33]. Thus, when using existing models of physical properties of SMA, empirical parameter fitting is necessary. Moreover, existing literature currently does not explicitly identify the limitations of knitted SMA under The main contributions of this paper include:

- Identification of the limitations of knitted SMA sheet actuators in Joule heating conditions
- Fabrication procedure for i-cord knitted SMA actuators, which do not share the limitation on uneven actuation
- Model verification for strain and resistance of single-strand SMA and corresponding empirical parameter fitting
- Combined electrical resistance, Joule heating, and mechanics model of i-cord knitted SMA actuators
- Experimental verification of resistance-strain relationships for i-cord knitted SMA actuators

II. I-Cord Knitted SMA Actuator

A. Fabrication of I-Cord knitted SMA actuator

An i-cord knit is traditionally a helical tube knitted in the round with two double-pointed needles, and was initially discovered by Elizabeth Zimmermann. An i-cord knitted SMA actuator utilizes this i-cord knit pattern to serve as the overall geometrical structure for SMA actuation. In order to create samples with knit loops of constant diameter, our i-cord knitted SMA actuators were fabricated using the four-needle Tulip i-cord knitter. Fig. 1 shows the fabrication process. A 200g weight was attached to the bottom of the knit to provide constant tension during the knitting process. The number of courses in the i-cord knits were kept constant by using four needles in the knitter, and the number of wales were varied for each sample by counting how many times a specific needle in the knitter created a loop. Once the i-cord knitted SMA was removed from the knitter by rotating the handle counter-clockwise, bind-off was performed by making the loose end go through the four unfinished knit loops. After bind-off, pulling the two ends ties off the knits securely. Then, 1A of current was supplied through the i-cord knitted SMA to further tighten the knits. If this procedure of running the current is skipped, the total strain achievable by the resultant i-cord knitted SMA actuator can significantly decrease. Finally, copper crimps were attached on both ends to create loops. These loops were later used to either hang the actuator on a frame or attach a weight to the actuator.

B. Rationale behind I-Cord Knitted SMA Actuator

I-cord knitted structures have various advantages compared to other knitted structures especially when it comes to Joule-heated knitted SMA actuators. These structures are axially symmetric (see Fig. 1(d)), making the resistance through every shortest path from one end of the actuator to the other end the same, and hence minimizing short-circuiting. As will be discussed in section IV-A, this allows every loop of the knitted structure to be heated equally unlike knitted SMA sheets. Further, since the I-cord is a cylindrical knit, there is no need to consider boundary conditions as every loop is connected to two neighboring loops, which is not the case for knitted SMA sheets.

TABLE I
Model Parameters

Martensite Fraction and Temperature Model	
$\mu+ = 78.9°C$	$\sigma+ = 11.2°C$
Resistivity Model	
$p_1 = 9.2\times10^{-7}\Omega m$	$\alpha_0 = 8.7\times10^{-7}\Omega m$
$p_2 = 8.4\times10^{-7}\Omega m$	$\alpha_1 = 4.8\times10^{-8}\Omega m°C^{-1}$
$p_3 = 0.2499\ °C^{-1}$	$\alpha_2 = -7.8\times10^{-9}\Omega m°C^{-2}$
$q_1 = 3.4\times10^{-8}\Omega m$	$\alpha_3 = 7.0\times10^{-10}\Omega m°C^{-3}$
$q_2 = 5.7\times10^{-10}\Omega m$	$\alpha_4 = -3.7\times10^{-11}\Omega m°C^{-4}$
$m_3 = 70\ °C$	$\alpha_5 = 1.2\times10^{-12}\Omega m°C^{-5}$
$n_3 = 3\ °C^{-1}$	$\alpha_6 = -2.5\times10^{-13}\Omega m°C^{-6}$
$T_{amb} = 24°C$	$\alpha_7 = 3.2\times10^{-16}\Omega m°C^{-7}$
	$\alpha_8 = -2.2\times10^{-18}\Omega m°C^{-8}$
	$\alpha_9 = 6.7\times10^{-21}\Omega m°C^{-9}$
Strain Model	
$E_a = 79$ GPa	$E_m = 31$ GPa
Electrical and Thermal Model	
$\rho = 6450\ kgm^{-3}$†	$h = 100\ Wm^{-2\circ}C^{-1}$
$L_0 = 0.004$ m*	$c = 836.8\ Jkg^{-1\circ}C^{-1}$†
$L_l = 0.002$ m*	$k = 18\ Wm^{-1\circ}C^{-1}$†
$d_0 = 0.000254$ m†	

Parameters in the first two models taken from [25]
**: Quantities determined empirically*
†: From manufacturer specifications

III. Model

A. Foundational Model for Single-strand SMA

For an individual SMA wire, we use a differential hysteresis model of a SMA wire adapted from [25] and [26]. The model equates martensite fraction (R_m) to temperature (T), strain (ϵ), and resistivity (ρ) of SMA, and it was used as an underlying foundation to derive the model for i-cord knitted SMA in the following section. The relationship between martensite fraction (R_m) and temperature (T) is computed by integrating Gaussian distribution functions in accordance with the general differential hysteresis model as follows:

$$h_{+/-}(u) = \frac{1}{2}\left[1 + \mathrm{erf}\left(\frac{u-\mu_{+/-}}{\sigma_{+/-}\sqrt{2}}\right)\right]$$

$$g_{+/-}(u) = \frac{1}{\sigma_{+/-}\sqrt{2\pi}}\exp\left(-\frac{(u-\mu_{+/-})^2}{2\sigma_{+/-}^2}\right)$$

$$\frac{dR_m}{dT} = \begin{cases} \frac{h_-(T)+R_m-1}{h_+(T)-h_-(T)}g_+(T), & \dot{T} \geq 0 \\ \frac{h_+(T)+R_m-1}{h_-(T)-h_+(T)}g_-(T), & \dot{T} < 0 \end{cases}, \ R_m(0) = 1 \tag{1}$$

Where $g(u)$ is the Gaussian distribution function with mean μ and variance σ^2 at temperature u and +/- represent increasing and decreasing. The martensite fraction is used

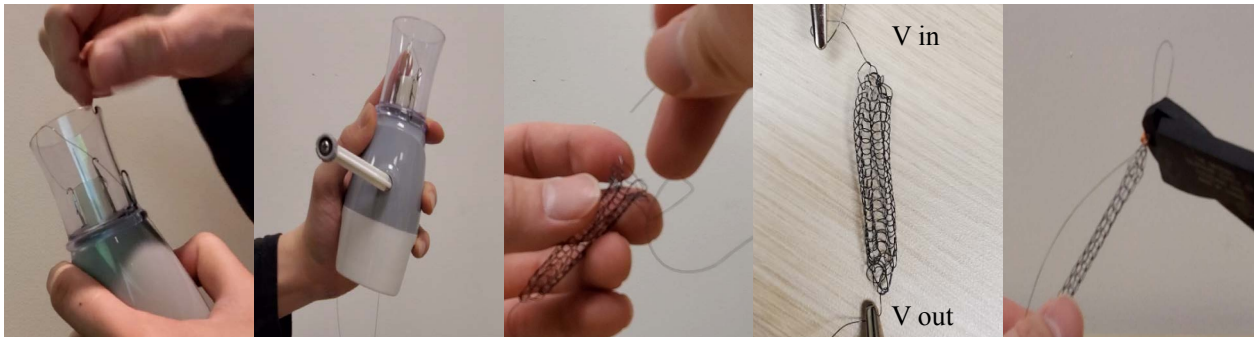

(a) (b) (c) (d) (e)

Fig. 1. Fabrication process of an i-cord knitted SMA actuator: (a) Attach NiTi wire into the Tulip i-cord knitter in anti-feeding direction (b) Rotate the handle clockwise and pull the weight downwards every time a knit loop is unlatched from the needles (c) After removing the i-cord knitted SMA by rotating the handle counter-clockwise, perform bind-off (d) Run 1A of current through the i-cord knitted SMA for 3 seconds in order to tighten the knits (e) Attach copper crimps to create loops on both ends

to calculate the tensile stress, σ using a variable sublayer model of stresses due to martensite and austenite [MPa] as shown in equation (2).

$$\sigma = (1 - R_m)\,\sigma_a + R_m \sigma_m \tag{2}$$

The overall resistance is calculated using

$$\frac{1}{R} = \frac{\pi d_0^2}{4L_0(1+2\epsilon)}\left[\frac{1-R_m}{\rho_A(T)} + \frac{R_m}{\rho_M(T)}\right] \tag{3}$$

$$\rho_A(T) = p_1 + p_2 \exp\left(-p_3\left(T - T_{\text{amb}}\right)\right) \tag{4}$$

$$\begin{aligned}\rho_M(T) = (q_1 - q_2 T')[1 + \text{erf}(\frac{T' - m_3}{n_3})] \\ + \sum_{i=0}^{i=9} \alpha_i (T' - T_{\text{amb}})^i \\ \textit{where } T' = \frac{13}{33}(T - T_{\text{amb}}) + T_{\text{amb}}\end{aligned} \tag{5}$$

where R is the overall resistance and $\rho_{A/M}$ are the resistivity values of the A/M Phase [Ωm], and p_{1-3}, $q_{1,2}$, m_3, n_3, and α_i ($i = 0, 1, ...9$) are constant parameters. Due to a discrepancy between the mathematical expression of ρ_M and its graph in [25], equation (5) was slightly modified from what was originally given from [25]. Since the mathematical expression gave unreasonably low ρ_M values for high temperatures, the expression was scaled differently so that $T' = 13(T - T_{amb})/33 + T_{amb}$. After this update, the resultant mathematical expression gave similar ρ_M values to what was given in the graph in [25].

The strain in the SMA wire is then determined by modeling the stress-strain relationship in terms of Young's modulus of the austenite, fully twinned martensite, partially twinned martensite, and detwinned martensite phases (E_a, E_m, E_T, and E_d), the yield strain of the twinned martensite (ε_m^y), and the minimum strain of the detwinned martensite (ε_m^d).

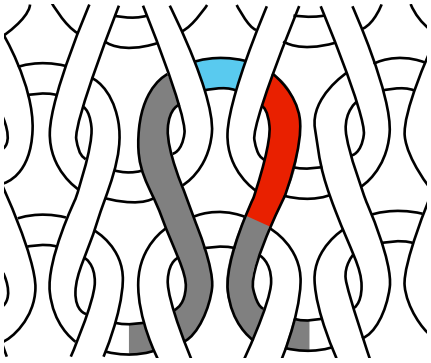

Fig. 2. Longitudinal (red) and lateral (blue) part of a unit knit cell

$$\epsilon = \begin{cases} \frac{\sigma}{[E_a - (E_a - E_m)R_m]}, & 0 \le \varepsilon < \varepsilon_m^y \\ \frac{\sigma + R_m(E_T - E_m)\varepsilon_m^y}{[E_a - (E_a - E_T)R_m]}, & \varepsilon_m^y \le \varepsilon < \varepsilon_m^d \\ \frac{\sigma + R_m\left[(E_T - E_m)\varepsilon_m^y + (E_d - E_T)\varepsilon_m^d\right]}{[E_a - (E_a - E_d)R_m]}, & \varepsilon_m^d < \varepsilon \end{cases} \tag{6}$$

B. Electrical and Thermal Model for I-Cord Knitted SMA

For an electrically activated SMA, the temperature rises due to Joule heating via standard heat conduction models. As a result, the temperature of the knit over time will depend on the bulk resistance of the knit. Because of the high level of symmetry in knitted structures, the entire i-cord knitted SMA actuator modeled as reflections and rotations of a quarter of a knit loop. Geometrically, [7] defined this quarter of a knit loop as a "unit knit cell." The unit knit cell is shown as the red and blue region in Fig. 2. We call the red part as the longitudinal part of a unit knit cell and the blue part as the lateral part of a unit knit cell.

Decomposing an i-cord knitted SMA actuator in this way enables us to model the knit as an electrical network of the longitudinal and lateral parts of a unit knit cell. Fig. 3 shows a simplified circuit diagram of the resistance model of an i-cord knitted SMA actuator. The variable n represents the number of wales, $R1$ is twice the resistance of the longitudinal part of a unit knit cell (shown as red in Fig. 2), and $R2$ is twice

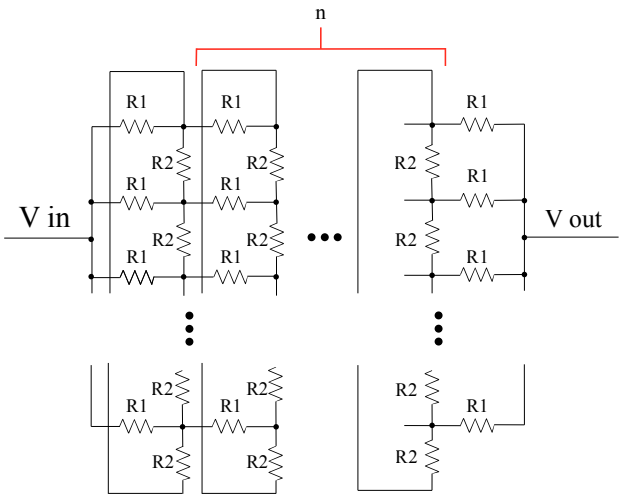

Fig. 3. Simplified circuit diagram of the resistance model of an i-cord knitted SMA actuator

the resistance of the lateral part of a unit knit cell (shown as blue in Fig. 2). It was assumed that all knit loops in the actuator are identical in dimensions. The bind-off on both ends (shown as the two columns on each end which are not included in n) of the actuator was assumed to have an equal length, and thus equal resistance, as the longitudinal part of a unit knit cell.

With this model, we apply Kirchhoff's voltage law (KVL) and Kirchhoff's current law (KCL) to obtain $16n + 24$ equations to determine the current flow on each resistor given a voltage input. and the bulk resistance of the system. The results is that all of the current passes through the horizontal ($R1$) resistors and none of the current passes through the vertical resistors ($R2$). Intuitively, this is reasonable in the circuit diagram as due to the perfect longitudinal symmetry in the circuit, every $R1$ resistor in each column is expected to carry the exact same current. Having current flow in any $R2$ resistors would either violate this symmetry or violate the KVL around a vertical loop that only contains $R2$ resistors.

Knowing how the current flows through an i-cord knitted SMA actuator, the temperature variation of the actuator can be separated into two components: Joule heating along the longitudinal part (which corresponds to $R1$) and conduction along the lateral part (which corresponds to $R2$). The Joule heating model can be directly derived from the lumped capacitance equation which was also used in [25],

$$\rho c \frac{\pi L_0 {d_0}^2}{4} \frac{dT}{dt} = R_1 I^2 - \pi d_0 L_0 h (T - T_{amb}) \qquad (7)$$

where ρ is the density, c is the specific heat, d_0 and L_0 are the cross-diameter and length of the undeformed wire, T is the temperature of the wire, T_{amb} is the ambient temperature, R_1 is twice the resistance of the longitudinal part, and h is the convective heat transfer coefficient of the wire.

The conduction equation can be directly derived from

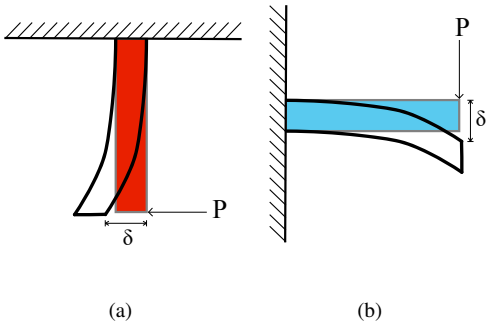

Fig. 4. Euler-Bernoulli beam bending approximation of the (a) longitudinal and (b) lateral part of a unit knit cell

Fourier's law

$$\rho c \frac{\pi L_l {d_0}^2}{4} \frac{dT}{dt} = -k \frac{\pi {d_0}^2}{4} \frac{dT}{dx} \qquad (8)$$

where L_l is the length of the lateral part of the unit knit cell, k is the conductivity of NiTi wire, and dx is the infinitesimal length parallel to the lateral part of the unit knit cell at each cross section. Values of k, ρ, c, and h were adopted from [34], [35].

After calculating the temperature variation of the longitudinal and lateral parts of the unit knit cell, the corresponding martensite fraction (R_m) can be calculated from equation (1). Using equations (4) and (5), the resistivity variation of the longitudinal and lateral parts of the unit knit cell can be obtained using the temperature and martensite fraction values. The resistance of the entire i-cord knitted SMA actuator could then be calculated by scaling it accordingly using Fig. 3.

C. Mechanics Model for I-Cord Knitted SMA

Finally, it remains to determine how the temperature-based phase changes in the individual wires behave when combined in a knit. Several load-extension models already exist for passive textile knits [36]–[43]. Our mechanics model for knitted SMA actuation follows the approach in [43] in which the longitudinal and lateral parts of a unit knit cell is considered to be two separate Euler-Bernoulli bending beams. In order to apply Euler-Bernoulli beam bending approximations, the NiTi wire is assumed to be inextensible. Although inextensibility is not necessarily an accurate assumption for NiTi due to its relatively large axial extension capability, it is used in the knit model because the extension of a knitted structure is assumed to be dictated by the change in the shape of the knit loops from bending [7].

Using linear small angle approximations to simplify the geometry of knitted structures, the longitudinal and lateral parts of a unit knit cell can be considered as a vertical and a horizontal cantilever beam as shown in Fig. 4. In the cantilever beam assumption, the tip deflection, δ, can be expressed as

$$\delta = \frac{PL^3}{3EI} \qquad (9)$$

where P is the applied load, L is the length of the beam,

E is the Young's modulus, and I is the cross-sectional area moment of inertia. Notice that Young's modulus, E, is the only quantity which can vary as the i-cord knitted SMA actuator is heated. Thus, the change in length of the i-cord knitted SMA actuator is mostly governed by the change in effective Young's modulus of the lateral part of each unit knit cell. The effective Young's modulus of NiTi can be expressed as a function of martensite fraction, R_m, using the variable sublayer model from [23].

$$\frac{1}{E} = \frac{1 - R_m}{E_a} + \frac{R_m}{E_m} \tag{10}$$

As discussed earlier for equation (6), E_a and E_m refer to the Young's modulus of NiTi in its austenite and martensite states. From the inextensibility assumption, Young's modulus of partially twinned and detwinned martensite phases (E_T and E_d respectively) were not considered. Using the variation in R_m from the electrical and thermal model, the effective change in Young's modulus, and thus the total strain achieved by the i-cord knitted SMA actuator can be obtained.

IV. Experimental Verification

A. Temperature Distribution for Knitted SMA

A uniform distribution of temperature across the knitted SMA actuators is desired since it allows for predictable, consistent deformations of the actuator. An uneven distribution of current and temperature could occur due to the knitted NiTi wires being uninsulated, leading to non-uniform contraction patterns. To investigate this effect in knitted SMA sheets, we compared rectangular vs i-cord knits of uninsulated NiTi wire. All samples were fabricated using 0.01 inch diameter wire (Dynalloy Flexinol LT 70°C wire, 0.010" diameter).

The rectangular samples were hand-knit using knitting needles of 2.25 mm diameter. Each knitted sample consisted of 7 wales and 23 courses. Care was taken to keep the width of each loop as even as possible to minimize the error associated with the manual fabrication process. The temperature distribution of the knitted SMA sheet as current was applied was recorded using an infrared thermal camera (FLIR C2). To measure the vertical and horizontal contraction across the sample, a video camera captured the deformation of the knitted sheet before and while a current was applied. Twelve evenly spaced markers were attached by knotting insulated copper wire to the sample; these served as landmarks between which the percent contraction could be calculated. Each marker was painted with white temperature resistant paint to provide enough contrast for a marker tracking system to detect the individual markers in the image frames. Additionally, the top and bottom of the sheet were tied to metal bars, so the attached load would be evenly distributed across the width of the sample. Surface plots representing the percent contraction observed between markers were generated by extracting each markers' pixel coordinates in the image and calibrating it to measure their displacements from one another.

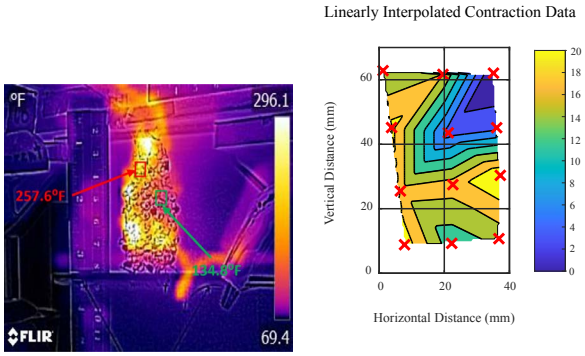

(a) (b)

Fig. 5. (a) Temperature distribution over knitted SMA sheet (b) Local percent contraction graph of the sheet

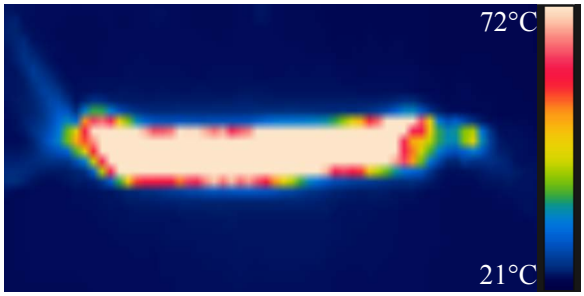

Fig. 6. Temperature distribution of an i-cord knitted SMA actuator under 1A of current

The results are shown in Fig. 5. An uneven distribution of temperature across the knitted SMA sheet can be seen in the thermal image and its effect on the sample's deformation. The distinct yellow C-like shape on the thermal image reached 125° C (257° F) while other areas remained lower than the 70° C (158° F) activation temperature. Surface plots of the sample show a higher percent contraction (yellow areas) between markers that corresponds to the same regions shown to reach higher temperatures in the thermal image. Additionally, the lower third of the sample achieved little contraction due to the activation temperatures not being reached in this region. This occurrence could be attributed to the fact that when the sample began contracting, specific loops across the uninsulated wire overlapped. As these electrical shorts occurred, the current traveled on the path of least resistance, causing only certain sections of the SMA knitted sheet to reach the activation temperature. This resulted in the nonuniform temperature distribution and deformation in the knitted samples.

In comparison, Fig. 6 shows the temperature distribution of an i-cord knitted SMA actuator (20 wales) when it is under 1A of current. As shown in the color bar on the right hand side of the figure, white and red denotes the higher temperature region, whereas black and blue denotes the lower temperature region. The i-cord knit is successful at producing a more even temperature distribution. Further, while the rectangular knit was able to achieve only 18% overall contraction, the i-cord knit was able to achieve 30%

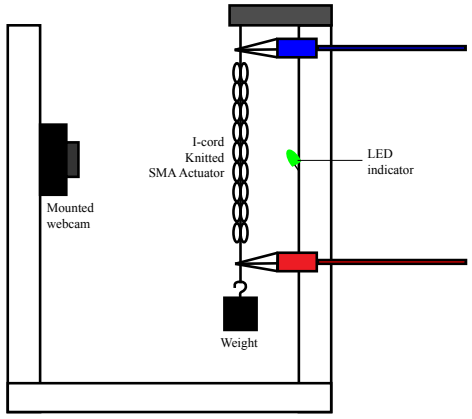

Fig. 7. Experiment setup used for single-strand SMA model verification

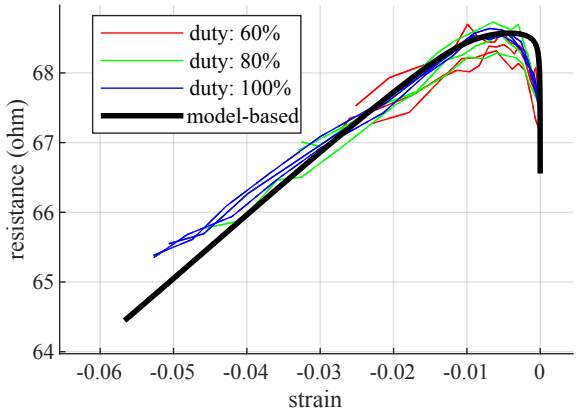

Fig. 8. Relationship between strain and resistance for single-strand SMA. The red, green, and blue lines show experimental data, whereas the black line shows model-based relationship in section III-A.

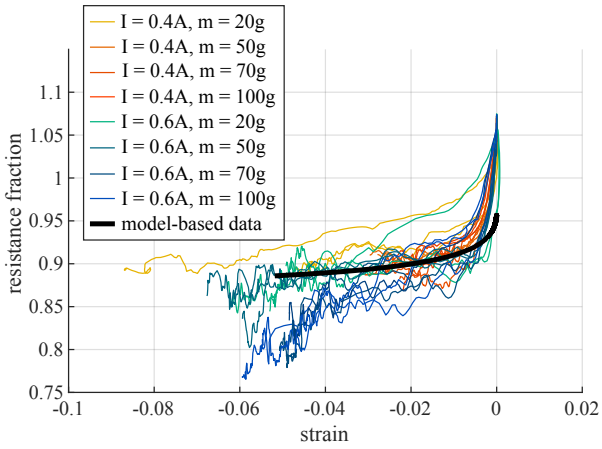

Fig. 9. Relationship between strain and non-dimensional resistance fraction for i-cord knitted SMA actuator. The non-black lines show experimental data, whereas the black line shows model-based relationship using section II.

overall contraction under the same conditions, indicating that the more even temperature distribution resulting from the cylindrical pattern improves the actuator efficiency.

B. Single-strand SMA Model Verification

In order to verify the strain-resistance relationship of single-strand NiTi wires, the same uninsulated NiTi wire of 0.01 inch diameter was cut into uniform lengths. Copper crimps were attached to both ends of the wire to create a loop to hang the wire on the frame and another loop to hang a 750g weight to the wire. The length between the copper crimp attachments were kept constant as 15 cm. As the SMA wire was stretched by the attached weight, pulse width modulation (PWM) current pulses were supplied for exactly four seconds using alligator clips attached to the copper crimps on both ends. An analog to digital converter (ADC) was used to measure the voltage drop across the SMA and across a reference series resistor to keep track of the varying resistance of the SMA. A webcam was mounted on the other side of the frame to record the contracting deformation of the SMA, whose videos were analyzed later to calculate the strain of the SMA wire using the Kanade-Lucas-Tomasi (KLT) feature-tracking algorithm [44]. The overall setup used in the experiment is shown in Fig. 7. The experiments were conducted by applying a PWM of five different duty cycles (20, 40, 60, 80, and 100%) and were repeated three times each using three different samples of the same length.

Fig. 8 shows the resultant relationship between strain and resistance of a single-strand SMA wire while PWM pulses are supplied. The red, green, and blue lines show experimental data, and the black line shows model-based relationship in section III-A. Note that only data from the high duty cycle trials (60, 80, and 100%) are shown in the plot because data from the other two lower duty cycles did not generate enough strain to make meaningful conclusions regarding the strain-resistance relationship of SMA. Negative strain values are used to denote a contraction from the original martensite phase. Note that the sign convention here is different from [25], in which positive strain was used to denote extension from the austenite phase. After adjusting the sign convention and scaling the resistance according to the 15cm samples used, it can be seen from Fig. 8 that the experimental data matches well with the model-based data for all duty cycles and trials. Importantly, the strain-resistance relationship is not a one-to-one relationship. This is consistent with the results from [25]. Thus, when resistance is used to estimate the strain of an SMA actuator, it will be necessary for the controller to take into account of other data such as rate of change of resistance or a thermal model-based estimation of the martensite fraction using how much heat energy has already been generated by supplying current and been lost by convective heat transfer.

C. I-cord Knitted SMA Model Verification

Using the fabrication method listed in section II-A, five i-cord knitted SMA actuators with different number of wales (8, 13, 17, 22, 28) were manufactured. A similar setup as the one in Fig. 7 was used to measure the strain and resistance of the I-cord knitted SMA actuators under different loads and input currents.

Fig. 9 shows the resultant relationship between strain and

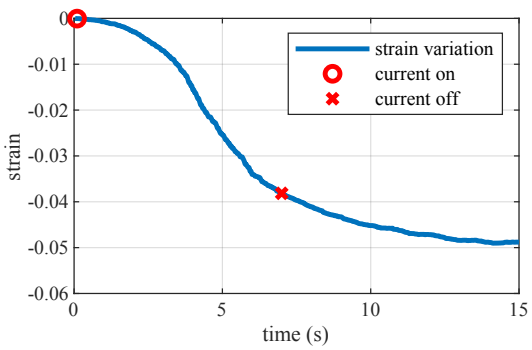

Fig. 10. Strain variation over time of an i-cord knitted SMA actuator with 28 wales, 0.6A of current, and 100g of weight. The red 'o' and 'x' indicate when current was turned on and off.

resistance fraction of an i-cord knitted SMA actuator. The black line shows the model-based relationship using the electric, thermal, and mechanics model outlined in section II. Resistance fraction is a non-dimensional quantity which was introduced to account for the difference in number of wales for different samples. The model-based data accurately predicts the overall trend of the resistance fraction and strain relationship for i-cord knitted SMA actuators. Since resistance is a function of material length, it had to be nondimensionalized by dividing the measured resistance by the resistance of the i-cord knitted SMA actuator at ambient temperature (T_{amb}). The resistance fraction goes above 1 when it is initially heated because resistivity of a fully martensite NiTi increases as its temperature increases. The model-based data in the figure, however, could not fully capture this initial spike in resistance fraction because it only includes data after it reaches 10°C above ambient temperature. The current austenite resistivity model from equation (4) uses an exponential decay function, and the resistivity value seems to be unreasonably high when the temperature of NiTi is close to ambient temperature.

There does seem to be some deviation of the experiments from the model for higher loads in the higher current scenario. We suspect this is due to friction in the knit. Because the knit includes many strands in contact with each other, individual strands in the knit may stretch or bend without a corresponding amount of contraction being reflected immediately in the knit. This hypothesis is corroborated by Fig. 10, where the knit continues to contract for a limited amount of time, even after the current is turned off, indicating that future mechanics models will also need to take into account some temporal effect.

V. Conclusion

In this paper, we identified the uneven temperature distribution, and thus uneven contractile actuation, of knitted SMA sheet actuators in Joule heating conditions. I-cord knitted SMA actuators, thanks to its axially symmetric geometry, have been suggested as a solution for this limitation, and the fabrication procedure of our i-cord knitted SMA actuators have been outlined. Existing models on physical properties of single-strand SMA have been modified and parameter-fitted to match the characteristics of our NiTi wire. Electrical model for i-cord knitted SMA actuators have been developed by creating a simplified circuit diagram of a network of resistors, and a thermal model using Joule heating and conduction was developed based on the results of the electrical model. A mechanics model for i-cord knitted SMA was also given which incorporates Euler-Bernoulli beam bending for the longitudinal and lateral parts of a unit knit cell. These models have been experimentally verified by comparing the resultant strain-resistance relationships.

The strain-resistance relationship, although is not a one-to-one relationship, is valuable in measuring the current actuation stage of an i-cord knitted SMA actuator with minimal apparatus. When used with the model that accurately predicts the electrical and mechanical properties of the actuator, simple resistance measurements across the actuator might be able to allow the controller to estimate its achieved strain. The proposed i-cord knitted SMA actuator is lightweight, have high power density, and can increase the contractile strain with its knitted geometry while overcoming the limitation of uneven distribution of temperature and actuation of existing knitting SMA actuators in Joule heating conditions. When used with a powerful controller that only requires resistance measurements, the actuator can be extremely useful especially for lightweight soft robots. The helical tube-like structure of the i-cord knitted SMA actuator can also offer new methods in supporting the overall soft structure of the robot, while preserving its high elasticity.

One of the greatest limitations of the i-cord knitted SMA actuator is, similar to any other SMA actuators, its relatively slow cooling time, which might make it unsuitable for applications to dynamic robots which require higher actuator bandwidth. An antagonistic setup of two actuators acting against each other might help solve this problem, or the SMA itself might have to be replaced with another smart material. Fortunately, the general electrical, thermal, and mechanics model proposed in this paper can also be applied to other smart materials arranged in the i-cord knit geometry, provided the correct parameters are inputted into the model. Future work involves better characterizing the knit and variations that would improve its actuation efficiency.

Acknowledgement

The authors would like to thank Addison Liu, Andrew Low, and Woohyuk Yang for assistance on prototyping the experimental setup, and Yuxuan Huang and Wei-Hsi Chen for discussions on modeling SMA.

References

[1] C. Rossi, J. Colorado, W. Coral, and A. Barrientos, "Bending continuous structures with SMAs: a novel robotic fish design," *Bioinspiration & Biomimetics*, vol. 6, no. 4, p. 045005, 2011.

[2] J.-E. Shim, Y.-J. Quan, W. Wang, H. Rodrigue, S.-H. Song, and S.-H. Ahn, "A smart soft actuator using a single shape memory alloy for twisting actuation," *Smart Materials and Structures*, vol. 24, no. 12, p. 125033, 2015.

[3] S. Yan, J. Zhang, M. Li, G. Alici, H. Du, R. Sluyter, and W. Li, "On-chip high-throughput manipulation of particles in a dielectrophoresis-active hydrophoretic focuser," *Scientific Reports*, vol. 4, p. 5060, 2014.

[4] F. Carpi, R. Kornbluh, P. Sommer-Larsen, and G. Alici, "Electroactive polymer actuators as artificial muscles: are they ready for bioinspired applications?" *Bioinspiration & Biomimetics*, vol. 6, no. 4, p. 045006, 2011.

[5] S. Shian, K. Bertoldi, and D. R. Clarke, "Dielectric elastomer based "grippers" for soft robotics," *Advanced Materials*, vol. 27, no. 43, pp. 6814–6819, 2015.

[6] H. Jin, E. Dong, M. Xu, C. Liu, G. Alici, and Y. Jie, "Soft and smart modular structures actuated by shape memory alloy (SMA) wires as tentacles of soft robots," *Smart Materials and Structures*, vol. 25, no. 8, p. 085026, 2016.

[7] J. Abel, J. Luntz, and D. Brei, "Two-dimensional analytical model and experimental validation of garter stitch knitted shape memory alloy actuator architecture," in *Smart Materials, Adaptive Structures and Intelligent Systems*, vol. 2, 2009, pp. 353–368.

[8] R. Granberry, K. Eschen, B. Holschuh, and J. Abel, "Functionally graded knitted actuators with niti-based shape memory alloys for topographically self-fitting wearables," *Advanced Materials Technologies*, vol. 4, no. 11, p. 1900548, 2019.

[9] R. Granberry, J. Abel, and B. Holschuh, "Active knit compression stockings for the treatment of orthostatic hypotension," in *Proceedings of the 2017 ACM International Symposium on Wearable Computers*, 2017, pp. 186–191.

[10] J. M. Hollerbach, I. W. Hunter, and J. Ballantyne, *A Comparative Analysis of Actuator Technologies for Robotics*. Cambridge, MA, USA: MIT Press, 1992, p. 299–342.

[11] K. Ikuta, M. Tsukamoto, and S. Hirose, "Shape memory alloy servo actuator system with electric resistance feedback and application for active endoscope," in *IEEE International Conference on Robotics and Automation*, 1988, pp. 427–430.

[12] J. A. Shaw and S. Kyriakides, "Thermomechanical aspects of NiTi," *Journal of the Mechanics and Physics of Solids*, vol. 43, no. 8, pp. 1243 – 1281, 1995.

[13] D. Chen and Q. Pei, "Electronic muscles and skins: a review of soft sensors and actuators," *Chemical Reviews*, vol. 117, no. 17, pp. 11 239–11 268, 2017.

[14] J. M. Jani, M. Leary, A. Subic, and M. A. Gibson, "A review of shape memory alloy research, applications and opportunities," *Materials & Design (1980-2015)*, vol. 56, pp. 1078–1113, 2014.

[15] H. Mehrabi and I. Aminzahed, "Design and testing of a microgripper with SMA actuator for manipulation of micro components," *Microsystem Technologies*, vol. 26, no. 2, pp. 531–536, 2020.

[16] J. Kyung, B. Ko, Y. Ha, and G. Chung, "Design of a microgripper for micromanipulation of microcomponents using SMA wires and flexible hinges," *Sensors and Actuators A: Physical*, vol. 141, no. 1, pp. 144 – 150, 2008.

[17] M. Kohl, B. Krevet, and E. Just, "SMA microgripper system," *Sensors and Actuators A: Physical*, vol. 97-98, pp. 646 – 652, 2002.

[18] J.-H. Lee, Y. S. Chung, and H. Rodrigue, "Long shape memory alloy tendon-based soft robotic actuators and implementation as a soft gripper," *Scientific reports*, vol. 9, no. 1, pp. 1–12, 2019.

[19] A. Hadi, A. Hassani, K. Alipour, R. Askari Moghadam, and P. Pourakbarian Niaz, "Developing an adaptable pipe inspection robot using shape memory alloy actuators," *Journal of Intelligent Material Systems and Structures*, vol. 31, no. 4, pp. 632–647, 2020.

[20] C. Mc Caffrey, T. Umedachi, W. Jiang, T. Sasatani, Y. Narusue, R. Niiyama, and Y. Kawahara, "Continuum robotic caterpillar with wirelessly powered shape memory alloy actuators," *Soft Robotics*, 2020.

[21] S. Karimi and B. Konh, "Self-sensing feedback control of multiple interacting shape memory alloy actuators in a 3D steerable active needle," *Journal of Intelligent Material Systems and Structures*, p. 1045389X20919971, 2020.

[22] G. M. Kamalakannan, G. K. Singh, and C. M. Ananda, "A multi-segment morphing system for a micro air vehicle using shape memory alloy actuators," *Defence Science Journal*, vol. 70, no. 1, pp. 3–9, 2020.

[23] K. Ikuta, M. Tsukamoto, and S. Hirose, "Mathematical model and experimental verification of shape memory alloy for designing micro actuator," in *IEEE Micro Electro Mechanical Systems*, 1991, pp. 103–108.

[24] K. Ikuta, "Micro/miniature shape memory alloy actuator," in *IEEE International Conference on Robotics and Automation*, 1990, pp. 2156–2161.

[25] S. M. Dutta and F. H. Ghorbel, "Differential hysteresis modeling of a shape memory alloy wire actuator," *IEEE/ASME Transactions on Mechatronics*, vol. 10, no. 2, pp. 189–197, 2005.

[26] D. R. Madill and D. Wang, "Modeling and l/sub 2/-stability of a shape memory alloy position control system," *IEEE Transactions on Control Systems Technology*, vol. 6, no. 4, pp. 473–481, 1998.

[27] N. T. Tai and K. K. Ahn, "Output feedback direct adaptive controller for a SMA actuator with a kalman filter," *IEEE Transactions on Control Systems Technology*, vol. 20, no. 4, pp. 1081–1091, 2012.

[28] *Effect of Geometric Design Parameters on Contractile SMA Knitted Actuator Performance*, ser. Smart Materials, Adaptive Structures and Intelligent Systems, vol. 2, 09 2017, v002T04A018.

[29] K. Eschen, J. Garcia-Barriocanal, and J. Abel, "In-situ strain- and temperature-control X-ray micro-diffraction analysis of nickel–titanium knitted architectures," *Materialia*, vol. 11, p. 100684, 2020.

[30] T. L. Buckner, R. A. Bilodeau, S. Y. Kim, and R. Kramer-Bottiglio, "Roboticizing fabric by integrating functional fibers," *Proceedings of the National Academy of Sciences*, vol. 117, no. 41, pp. 25 360–25 369, 2020.

[31] J. Kennedy and K. Fontecchio, "Textile-based shape memory alloy locomotive robot," in *International Conference on Control, Automation and Robotics (ICCAR)*, 2017, pp. 237–241.

[32] M.-W. Han and S.-H. Ahn, "Blooming knit flowers: Loop-linked soft morphing structures for soft robotics," *Advanced Materials*, vol. 29, no. 13, p. 1606580, 2017.

[33] J. Uchil, K. Mahesh, and K. G. Kumara, "Electrical resistivity and strain recovery studies on the effect of thermal cycling under constant stress on R-phase in NiTi shape memory alloy," *Physica B: Condensed Matter*, vol. 324, no. 1-4, pp. 419–428, 2002.

[34] *Nitinol technical properties*, Johnson Matthey.

[35] S. Yang and G. Dui, "Temperature analysis of one-dimensional NiTi shape memory alloys under different loading rates and boundary conditions," *International Journal of Solids and Structures*, vol. 50, no. 20-21, pp. 3254–3265, 2013.

[36] R. Postle and D. Munden, "25—analysis of the dry-relaxed knitted-loop configuration: Part II: Three-dimensional analysis," *Journal of the Textile Institute*, vol. 58, no. 8, pp. 352–365, 1967.

[37] G. Leaf, "4—models of the plain-knitted loop," *Journal of the Textile Institute Transactions*, vol. 51, no. 2, pp. T49–T58, 1960.

[38] K.-F. Choi and T.-Y. Lo, "An energy model of plain knitted fabric," *Textile research journal*, vol. 73, no. 8, pp. 739–748, 2003.

[39] D. Semnani, M. Latifi, S. Hamzeh, and A. Jeddi, "A new aspect of geometrical and physical principles applicable to the estimation of textile structures: an ideal model for the plain-knitted loop," *Journal of the Textile Institute*, vol. 94, no. 3-4, pp. 202–211, 2003.

[40] A. Kurbak and O. Ekmen, "Basic studies for modeling complex weft knitted fabric structures part i: A geometrical model for widthwise curlings of plain knitted fabrics," *Textile Research Journal*, vol. 78, no. 3, pp. 198–208, 2008.

[41] S. De Jong and R. Postle, "34—an energy analysis of the mechanics of weft-knitted fabrics by means of optimal-control theory part i: The nature of loop-interlocking in the plain-knitted structure," *Journal of the Textile Institute*, vol. 68, no. 10, pp. 307–315, 1977.

[42] W. Shanahan and R. Postle, "23—a theoretical analysis of the tensile properties of plain-knitted fabrics. part i: The load-extension curve for fabric extension parallel to the courses," *Journal of the Textile Institute*, vol. 65, no. 4, pp. 200–212, 1974.

[43] H. Hong, M. De Araujo, R. Fangueiro, and O. Ciobanu, "Theoretical analysis of load-extension properties of plain weft knits made from high performance yarns for composite reinforcement," *Textile research journal*, vol. 72, no. 11, pp. 991–996, 2002.

[44] C. Tomasi and T. Kanade, "Detection and tracking of point features," School of Computer Science, Carnegie Mellon University, Tech. Rep. CMU-CS-91-132, 1991.